Semiconductor Science and Technology

PAPER

Mid-wave interband cascade infrared photodetectors based on GaInAsSb absorbers

To cite this article: Lin Lei *et al* 2016 *Semicond. Sci. Technol.* **31** 105014

Mid-wave interband cascade infrared photodetectors based on GaInAsSb absorbers

Lin Lei,[1,2] Lu Li,[1] Hossein Lotfi,[1] Yuchao Jiang,[1] Rui Q. Yang,[1] Matthew B. Johnson[2], Dmitri Lubyshev,[3] Yueming Qiu[3], Joel M Fastenau[3] and Amy W. K. Liu[3]

[1]School of Electrical and Computer Engineering, University of Oklahoma, Norman, Oklahoma, USA 73019

[2]Department of Physics and Astronomy, University of Oklahoma, Norman, Oklahoma, USA, 73019

[3]IQE Inc., 119 Technology Drive, Bethlehem, Pennsylvania, USA, 18015

Abstract

In this work, we report the demonstration of quaternary GaInAsSb-based mid-wavelength infrared (MWIR) photodetectors with cutoff wavelengths longer than 4 μm at 300 K. Both interband cascade infrared photodetector (ICIP) with a three-stage discrete absorber architecture and conventional one-stage detector structures have been grown by molecular beam epitaxy and investigated in experiments for their electrical and optical properties. High absorption coefficient and gain were observed in both detector structures. The three-stage ICIPs had superior carrier transport over the one-stage detectors. A detectivity as high as 1.0×10^9 cm·Hz$^{1/2}$/W was achieved at 3.3 μm for both one- and three-stage detectors under zero bias at 300 K. The implications of these results are discussed along with potential of GaInAsSb-based ICIPs for high-speed applications.

Keywords: GaInAsSb alloy, infrared, interband cascade, photodetector, mid-wavelength.

I. Introduction

Interband cascade (IC) structures have been explored for constructing multi-stage infrared (IR) photodetectors with the advantage of circumventing the finite diffusion length limitation in narrow bandgap photodetectors,[1] leading to improved high-temperature and high-speed operation.[1-5] By using InAs/GaSb type-II superlattices (SLs) as the absorbers, IC IR photodetectors (ICIPs) have been demonstrated over a wide wavelength range from short-wave (SW) to very long-wave (VLW) (2.9 to 16 μm).[1-7] InAs/GaSb type-II SL absorbers have certain advantages, such as low tunneling current (with a relatively large effective mass insensitive to the SL bandgap) and the suppression of Auger recombination.[8] However, the drawback of type-II SL detectors is their relatively small absorption coefficient. This issue can be alleviated by using bulk semiconductor materials such as GaInAsSb as the absorbers. In contrast to type-II SL where electrons and holes are mainly located in different layers, GaInAsSb absorber allows even distribution of electrons and holes in the same layer and interfaces are eliminated. Consequently, high optical absorption coefficient and responsivity can be achieved with relatively thin GaInAsSb absorbers, which is desirable to obtain fast response without compromising signal strength. Additionally, the use of GaInAsSb absorbers, instead of type-II SL absorbers with many interfaces, drastically reduces shutter movements during their MBE growth, which should make the mechanical parts of MBE last significantly longer without maintenance. The bandgap of $Ga_{1-x}In_xAs_ySb_{1-y}$ can be tailored by changing the composition to cover from 0.25 to 0.73 eV, while keeping it lattice matched to GaSb.[9] Although the growth of quaternary GaInAsSb alloys is challenging, especially in immiscibility regions,[10,11] they have been used in infrared optoelectronic devices such as lasers,[12,13] thermophotovoltaics,[14,15] and infrared photodetectors.[16-18] Nevertheless, to the best of our knowledge, GaInAsSb detectors have not been reported in MWIR wavelength region beyond 3 μm even though the growth of thick GaInAsSb layer had been demonstrated on GaSb substrates with substantial strain and improved material quality.[13,19,20] Also, until this work, there has not been any study reported with bulk GaInAsSb material in ICIPs. In this paper, we present our initial investigation of ICIPs with quaternary GaInAsSb absorbers with a cutoff wavelength beyond 4 μm at 300 K. High absorption coefficients (compared to type-II SL at similar wavelength) and gain have been observed from these initial GaInAsSb ICIPs.

II. Device structures and material growth

Two detector structures were designed with quaternary $Ga_{0.44}In_{0.56}As_{0.5}Sb_{0.5}$ absorbers, which are lattice matched to the GaSb substrate and with a bandgap of about 0.29 eV at 300 K,[9] corresponding to a cutoff wavelength of 4.3 μm. One structure is three-stage ICIP (ICIP-3) that has three cascade stages with thicknesses of individual absorbers designed as 260, 365 and 575 nm, respectively, as shown in Fig. 1. Thicker absorbers in the optically deeper stages are to ensure the photocurrent matching. The other one is one-stage detector (ICIP-1), in which the absorber thickness is 1,200 nm, equal to the total absorber thickness of ICIP-3. The *p*-type absorbers (p=2.8×10^{16} cm^{-3}) were sandwiched between the electron and hole barrier in each stage, as shown in Fig. 1. The hole barrier is composed of digitally graded three InAs/Al(In)Sb quantum wells (QWs) with well layer thickness of 83, 72, and 65 Ȧ, respectively. The electron barrier is composed of digitally graded seven GaSb/AlSb QWs with well layer thickness of 10, 12, 15, 19, 25, 36 and 53 Ȧ, respectively, which is significantly thicker than the electron barrier with fewer

GaSb/AlSb QWs in our previous ICIPs[1,2] and should be sufficient to force electrons move towards the preferred direction.

The ICIP structures were grown on nominally undoped *p*-type GaSb substrates at IQE Inc. in an Oxford-VG V-100 solid source MBE tool using a production epitaxial growth process developed specifically for Sb-based materials. Group V (As, Sb) fluxes were controlled by valved cracker cells, while the group III molecular beams (In, Ga, Al) were produced via SUMO or conical effusion cells. Substrate growth temperatures for the bulk absorber and barrier QW sections ranged from 400 to 500°C, depending on the layer alloys and position within the structure. Additional details of the MBE configuration and *in situ* control tools have been previously described.[21,22] The undoped GaSb substrates were (100) with a miscut orientation of <0.5° and an epi-ready surface. Both ICIP structures are in the reverse illumination configuration[4], in which the hole barrier is close to the top surface and the light is incident on this top surface (Fig. 1).

The crystalline quality of the ICIP wafers was investigated using high resolution x-ray diffraction (HRXRD), as shown in Fig. 2. The full width at half maximum (FWHM) of the measured main peak are 38 and 21 arc seconds for one- and three-stage wafers, respectively, indicating very good structural quality for both wafers, with the three-stage wafer being somewhat better. The one-stage wafer had a small compressive strain (810 ppm), while the three-stage wafer had a small tensile strain (-520 ppm). From the inset HRXRD, multiple adjacent peaks beside substrate peak may indicate somewhat different compositions of the GaInAsSb alloys caused by small deviations from the targeted alloy composition during the MBE growth. Both wafers had surface defect densities lower than 1×10^3 cm^{-2} under optical microscope with defect size in the range of 1.3 to 50 μm^2.

After the growth, wafers were processed into square mesa detectors with dimensions from 50 to 1000 μm using conventional contact UV photolithography and wet etching. A two-layer passivation (Si_3N_4 then SiO_2) was RF sputtered deposited for improving overall stress management and minimizing pin holes in passivation layers. Ti/Au top and bottom contacts were also sputter deposited and then the devices were wire bonded for characterization.

III. Results and discussion

A. Electrical characteristics

The electrical characteristics of detectors from both wafers were examined over a wide range of temperatures (78 to 340 K). The dark current densities J_d of three-stage ICIPs are lower than the one-stage devices for each temperature from 78 K to 340 K, as shown in the Fig. 3 (a). This agrees with theoretical projections for thin individual absorbers and multiple stages.[23] Dark current densities in these GaInAsSb ICIPs are generally higher than those observed in our type-II SL ICIPs with similar cutoff wavelength.[24] For example, the dark current densities are 2.3×10^{-4} and 2.0×10^{-5} A/cm^2 for one- and three-stage ICIPs at 50 mV reverse bias at 78 K, respectively. One possible reason for this behavior is the small effective mass that might cause excessive leakage current (similar problems are observed in mercury cadmium telluride (MCT) detectors).[25] Another factor for high dark current density is a possible additional leakage channel with a relatively low shunt resistance. This is evident at a low bias region (<100 mV) and reverse bias at low temperatures (<200 K),[26] where the effective resistances of the detectors are large so that the impact of the shunt resistance in parallel is more significant. Under a high forward bias or at high temperatures (>200 K), other current components such as the diffusion current and recombination current exponentially increase and become more dominant than the shunt current via the leakage channel. The extracted product of dynamic resistance (R_D) and device area (A) is plotted in Fig. 3(b), which shows R_DA peaked at a reverse bias for high temperatures. This suggests that the carrier transport at high temperatures is more diffusion-dominant at low reverse bias. The shunt resistance plays a more dominant role at low temperatures and limits the value of R_0A (R_DA at zero bias voltage). For example, the value of R_0A for all devices was less than 4,000 $\Omega\cdot cm^2$ at 78 K. Hence, the Johnson noise limited detectivities are relatively small at low temperatures. At higher temperatures (above 200 K), dark currents converge at a high forward bias, with a constant series resistance (~5 Ω) indicating a good ohmic contact, as shown in Fig 3 (b). This series resistance is significantly smaller than that for this device at 300 K (>100 Ω). This series resistance may have some effect on accurate determination of certain properties (*i.e.* responsivity and Johnson-noise limited detectivity) for large size devices (R_0<10 Ω) at the higher temperature (>300 K). Hence, the value of this series resistance was subtracted in the value of R_0A for devices in Fig. 4.

Generally, because of shorter individual absorbers and multiple stages, the value of R_0A is significantly higher in three-stage ICIPs than in one-stage detectors at every temperature. Also, their R_0A values are less sensitive to the device size for three-stage devices, as shown in Fig. 4, where R_0A is plotted as the perimeter to area ratio (P/A) at high temperatures (see Fig. 4(b)). From 200 K up to 340 K, R_0A was nearly independent on the device size for three-stage ICIPs; and its size dependence was also weak for one-stage devices. These observations suggest that the leakage current might be from bulk defects. This is reflected by small activation energies that were extracted from devices, as show in Fig. 4 (a). The activation energy was obtained by an Arrhenius plot of device R_0A over the temperature range with the equation:

$$\frac{1}{R_0 A} \approx Ce^{-\frac{E_a}{k_B T}} \tag{1}$$

where E_a, T, k_B and C are the activation energy, temperature (K), Boltzmann constant and fitting prefactor, respectively. As show in Fig. 4 (a), a small activation energy of 30 meV is extracted from devices at low temperatures, which is indicative of surface leakage or defect-assisted tunneling currents. In the high temperature range (200-340 K), the extracted activation energies are 280 meV for three-stage and 260 meV for one-stage detectors. These values fall between the device bandgap (E_g=370 meV at 78 K) and the half-bandgap value. This suggests the existence of the Shockley-Read-Hall (SRH) recombination centers which, even though localized in the bulk materials, become dominant paths for tunneling and recombination current under certain conditions,[27,28] and contribute significantly to leakage current over the entire temperature range.

B. Optical characteristics

The photo-response spectra of devices at various temperatures were measured using a FTIR spectrometer and calibrated with an 800 K blackbody source (aperture diameter 1.52 cm). The cutoff wavelength is 3.7 (3.6) µm at 78 K and extends to 4.6 (4.5) µm at 300 K for the one-stage (three-stage) detectors. Figure 5 (a) displays the responsivity for both one- and three-stage detectors (at 50 mV) in a temperature range from 78 to 340 K. The responsivity in both detectors is bias dependent at all temperatures, which might be caused by an undesirable barrier[4,5,29,30] in the carrier transport path. For a clear illustration, the responsivity at a wavelength (λ) of 3.3 μm is shown in Fig. 5 (b) for devices at 0 and 50 mV, and the bias dependence is shown in Fig. 5 (c) for both one-stage and three-stage devices at various temperatures. At low temperatures (78 to 125 K), devices from both wafers reached the maximum response at a reverse bias voltage of 50 mV. However, the responsivity for three-stage ICIPs is less sensitive to bias voltage, and is nearly unchanged with the bias voltage at high temperatures (>250 K), where the thermal energy could be sufficient to assist carriers to overcome the unintended barrier. In contrast, one-stage devices have strong responsivity dependence on bias over the entire range of temperatures and requires higher reverse bias to reach the maximum as the temperature increases (Fig. 5 (c)). For instance, at 300 K, the responsivity at 3.3 μm for the one-stage device increases from 0.68 A/W at zero-bias to the maximum of 0.92 A/W near 150 mV (an increase of 35%). These large variations and the requirement of the higher bias voltage to reach peak responsivity for the one-stage device at high temperatures can be explained by the reduction of carrier diffusion length shorter than the absorber thickness (1.2 μm). Because of thinner individual absorbers (<0.6 μm) in the three-stage devices, efficient collection of photogenerated carriers is maintained over the whole operating temperature range. This is supported by the continuous increase of responsivity with the temperature for the three-stage devices, as shown in Fig. 5 (b) and (c). We note that with the narrowing of the bandgap, the responsivity of the one-stage device at a reverse bias also increased when temperature was raised from 78 to 300 K, but at a slower percentage change, and then reduces from 300 to 340 K. These results demonstrate that multiple stage ICIPs with thin absorbers have superior carrier transport over a one-stage device.

Additionally, an unusual temperature dependent responsivity was observed for the one-stage detectors under zero bias, as shown in Fig. 5(b). It decreases when temperature increases from 125 to 200 K, and then increased again with temperature up to 300 K. This behavior is not yet understood. Furthermore, after reaching its peak value, the responsivity sharply decreases with further increase of the reverse bias voltage in one-stage detectors, as shown in Fig. 5 (c). This behavior is also observed for three-stage devices at low temperatures, but at substantially small scales, however, similar behavior was never observed in our previous type-II SL photodetectors with either single or multiple stages. Similar responsivity dependence on bias voltage are observed by other groups in type-II SL[29] and MCT[30] photodetectors, for which trap-assisted tunneling is thought to be possibly responsible. Currently in this work, it is not clear whether the underlying mechanism is specifically related to the GaInAsSb absorber or to defect-assisted tunneling. These possible mechanisms will be investigated in the future.

Assuming that all photon-generated electrons are collected, the absorption coefficient, α, can be estimated from the device responsivity:

$$R_i(\lambda)\frac{1.24}{\lambda} = \eta(\lambda) = (1-R)(1-e^{-\alpha(\lambda)d}) \quad , \qquad (2)$$

where R_i is the responsivity, η is the external quantum efficiency, R is the reflectance at the device surface, and d is the absorber thickness. Considering that the photocurrent was determined by the first absorber (the thinnest one), the absorption coefficient is extracted and plotted in Fig. 6 along with the experimental result obtained from a transmission measurement on a piece of the one-stage wafer. For most of the measured region, the absorption coefficient extracted from the responsivity is significantly higher than the typical value (2000-3000 cm^{-1}) in type-II SLs, and also substantially higher than the experimental value determined from the transmission measurement as shown also in Fig. 6. For example, the absorption coefficient is 6,200 and 7,500 cm^{-1} at 3.3 μm based on responsivity for one- and three-stage devices at 300 K, which is higher than the experimental value of 4,900 cm^{-1} obtained from the transmission measurement. Also included in Fig. 6 is the theoretically calculated absorption coefficient based on a model[31] and the optical effective mass[32] including nonparabolic effects calculated with an eight-band model,[33] where a band gap of 0.3 eV was used for GaInAsSb absorber. The theoretically calculated result for α agrees well with the experimental value obtained from transmission measurement for photon energy near the bandgap up to 0.4 eV. The higher absorption coefficient extracted from the device responsivities, compared with the result obtained from the transmission measurement, suggests a gain exceeding unity. According to photoconductive theory,[34] the photoconductive gain is determined by the ratio of the carrier lifetime (τ) to the transit time (τ_t), which can be larger than 1 when the carrier lifetime is longer than the transit time. The ICIPs with short absorbers can be viewed as photoconductors, especially under a bias, in which carrier transit time might be substantially shorter than the carrier lifetime, resulting in a gain exceeding unity. This high gain was not observed from our previous ICIPs[1,2] where the electron barriers were thinner compared to the electron barriers in these GaInAsSb ICIPs. However, high gains (>5) have been reported for type-II SL detectors.[35,36] At this moment, we do not fully understand what was responsible for these gains, further effort is required to investigate these phenomena.

To further evaluate the device performance, the normalized detectivity, D^*, is determined according to the following equation

$$D^* = \frac{R_i}{\sqrt{\frac{4k_BT}{R_DA} + \frac{2qJ_d}{N_s}}} \quad , \tag{4}$$

for devices based on their responsivities and electrical properties by considering Johnson noise and shot noise, as plotted in Fig. 7. In Eq. (4), N_s is the number of stages in a device. The detectivities for the one- and three-stage detectors at low temperatures were not very high (1.8×10^{11} and 1.1×10^{11} cm·Hz$^{1/2}$/W at 3.3 µm and 78 K), they were limited by small R_0A values at low temperature, as discussed earlier. At 300 K, both one- and three-stage detectors had Johnson-noise limited detectivities of 10^9 cm·Hz$^{1/2}$/W at 3.3 µm under zero-bias voltage, which is comparable to the values obtained for type-II SL ICIPs with a similar cutoff wavelength[24] and for InAsSb nBn detectors with a 2-µm-thick absorber and cutoff wavelength near 4.5 µm at 300 K[37]. Under low reverse bias at 300 K, the device resistance increases by bias, as shown in Fig. 3 (b), resulting in an increase of D^*, as shown in Fig. 7 (b). In fact, D^* is somewhat higher in the one-stage device than that in the three-stage ICIP, because of the substantial increased responsivity in the one-stage device with the reverse bias. Here the benefit of ICIPs in terms of D^*, is not clearly observed, mostly because the R_0A values of the three-stage detectors was significantly lower than the theoretical projections for the ideal ICIPs[23] (*i.e.* transport is diffusion-limited and the diffusion length is longer than the absorber thickness), where R_0A in the three-stage ICIP would be about 10 times larger than that in the one-stage device. Issues such as leakage current associated with imperfect device passivation and bulk defects are the main reasons for the underperformance of the three-stage ICIPs presented in this work. When the total absorber thickness is equal for a multiple stage ICIP and a conventional one-stage detector, if the carrier transport is not dominated by diffusion, the expected high resistance with the discrete absorber architecture will not be achieved, resulting in a detectivity lower than theoretically projected. However, the total absorber thickness does not have to be equal, especially when the diffusion length is significantly shorter than the absorption length ($=1/\alpha$). In such a case, an ICIP can have more cascade stages with the total absorber thickness significantly longer than the diffusion length and the single absorber thickness of the conventional detector. Consequently, the device resistance of an ICIP can be significantly higher so that its D^* can exceed that for a single-stage detector.

IV. Summary

MWIR detectors have been demonstrated at temperatures up to 340 K based on absorbers composed of the quaternary GaInAsSb alloy in both a discrete absorber architecture and a conventional single absorber structure. Absorption coefficients (e.g. ~5000 cm^{-1} at 3.3 μm) significantly higher than the typical value (2000-3000 cm^{-1}) in type-II SLs are observed. Additionally, gain factors exceeding unity are observed in both structures, which will be the subject of further investigation. Johnson noise limited detectivity for both one- and three-stage detectors reached 10^9 cm·Hz$^{1/2}$/W at 300 K, comparable to type-II SL photodetectors with similar cutoff wavelengths. Nevertheless, the exploration of GaInAsSb-based MWIR photodetectors, particularly with the discrete absorber architecture, is in the preliminary phase and there are aspects that need to be understood and studied further. ICIPs with GaInAsSb absorbers will have potential advantages for high-speed applications with both high absorption coefficient and detectivity.

Acknowledgments

The authors are grateful to Hao Ye for helpful discussions on the characterization of the samples. This work was supported in part by AFOSR under Award FA9550-15-1-0067.

References

[1] R. Q. Yang, Z. Tian, Z. Cai, J. F. Klem, M. B. Johnson, and H. C. Liu, J. Appl. Phys. **107,** 054514 (2010).

[2] Z. Tian, R. T. Hinkey, R. Q. Yang, D. Lubyshev, Y. Qiu, J. M. Fastenau, W. K. Liu, and M. B. Johnson, J. Appl. Phys. **111,** 024510 (2012).

[3] N. Gautam, S. Myers, A. V. Barve, B. Klein, E. P. Smith, D. R. Rhiger, L. R. Dawson, and S. Krishna, Appl. Phys. Lett. **101,** 021106 (2012).

[4] H. Lotfi, L. Lei, L. Li, R. Q. Yang, J. C. Keay, M. B. Johnson, Y. Qiu, D. Lubyshev, J. M. Fastenau, and A. W. K. Liu, Opt. Eng. **54,** 063103 (2015).

[5] H. Lotfi, L. Li, L. Lei, Y. Jiang, R. Q. Yang, J. F. Klem, and M. B. Johnson, J. Appl. Phys. **119,** 023105 (2016).

[6] H. Lotfi, L. Li, H. Ye, R. T. Hinkey, L. Lei, R. Q. Yang, J. C. Keay, T. D. Mishima, M. B. Santos, and M. B. Johnson, Infrared Phys. Technol. **70,** 162 (2015).

[7] Z.-B. Tian, S. E. Godoy, H. S. Kim, T. Schuler-Sandy, J. A. Montoya, and S. Krishna, Appl. Phys. Lett. **105,** 051109 (2014).

[8] H. Mohseni, V. I. Litvinov, and M. Razeghi, Phys. Rev. B **58,** 15378 (1998).

[9] I. Vurgaftman, J. R. Meyer, and L. R. Ram-Mohan, J. Appl. Phys. **89,** 5815 (2001).

[10] M. J. Cherng, H. R. Jen, C. A. Larsen, G. B. Strigfellow, H. Lundt, and P. C. Taylor, J. Cryst. Growth **77,** 408 (1986).

[11] O. Kentaro, Jpn.J. Appl. Phys. **21,** L323 (1982).

[12] H. K. Choi, S. J. Eglash, and G. W. Turner, Appl. Phys. Lett. **64,** 2474 (1994).

[13] C. Lin, M. Grau, O. Dier, and M.-C. Amann, Appl. Phys. Lett. **84,** 5088 (2004).

[14] C. A. Wang, H. K. Choi, S. L. Ransom, G. W. Charache, L. R. Danielson, and D. M. DePoy, Appl. Phys. Lett. **75,** 1305 (1999).

[15] M. W. Dashiell, J. F. Beausang, H. Ehsani, G. J. Nichols, D. M. Depoy, L. R. Danielson, P. Talamo, K. D. Rahner, E. J. Brown, S. R. Burger, P. M. Fourspring, W. F. TopperJr, P. F. Baldasaro, C. A. Wang, R. K. Huang, M. K. Connors, G. W. Turner, Z. A. Shellenbarger, G. Taylor, J. Li, R. Martinelli, D. Donetski, S. Anikeev, G. L. Belenky, and S. Luryi, IEEE Trans. Electron Devices **53,** 2879 (2006).

[16] M. H. M. Reddy, J. T. Olesberg, C. Cao, and J. P. Prineas, Semicond. Sci. Technol. **21,** 267 (2006).

[17] H. Shao, A. Torfi, W. Li, D. Moscicka, and W. I. Wang, J. Cryst. Growth **311,** 1893 (2009).

[18] B. Zhang, T. Zhou, H. Jiang, Y. Ning, and Y. Jin, Electron. Lett. **31,** 830 (1995).

[19] A. Yildirim and J. P. Prineas, J. Vac. Sci. Tech. B: Microelectronics and Nanometer Structures **31,** 03C125 (2013).

[20] C. Lin and A. Z. Li, J. Cryst. Growth **203,** 511 (1999).

[21] D. Lubyshev, Y. Qiu, J. M. Fastenau, A. W. K. Liu, E. J. Koerperick, J. T. Olesberg, and J. D. Norton, Proc. SPIE **8268,** 82681A (2012).

[22] J. M. Fastenau, D. Lubyshev, Y. Qiu, A. W. K. Liu, E. J. Koerperick, J. T. Olesberg, and D. Norton Jr, Infrared Phys. Technol. **59,** 158 (2013).

[23] R. T. Hinkey and R. Q. Yang, J. Appl. Phys. **114,** 104506 (2013).

[24] H. Lotfi, L. Li, L. Lei, H. Ye, S. M. S. Rassel, Y. Jiang, R. Q. Yang, T. D. Mishima, M. B. Santos, J. A. Gupta, and M. B. Johnson, Appl. Phys. Lett. **108,** 201101 (2016).

[25] A. Rogalski, Rep. Prog. Phys. **68,** 2267 (2005).

[26] S. Banerjee and W. A. Anderson, Appl. Phys. Lett. **49,** 38 (1986).

[27] E. H. Aifer, S. I. Maximenko, M. K. Yakes, C. Yi, C. L. Canedy, I. Vurgaftman, E. M. Jackson, J. A. Nolde, C. A. Affouda, M. Gonzalez, J. R. Meyer, K. P. Clark, and P. R. Pinsukanjana, Proc. SPIE **7660,** 76601Q (2010).

[28] B. Monemar and B. E. Sernelius, Appl. Phys. Lett. **91,** 181103 (2007).

[29] J. E. A. DeCuir, G. P. Meissner, P. S. Wijewarnasuriya, N. Gautam, S. Krishna, N. K. Dhar, R. E. Welser, and A. K. Sood, Opt. Eng. **51,** 124001 (2012).

[30] M. Kopytko and A. Rogalski, Prog. Quant. Electron. **47,** 1 (2016).

[31] S. L. Chuang, *Physics of Photonic Devices* (Wiley Publishing, 2009).

[32] Y. B. Li, R. A. Stradling, T. Knight, J. R. Birch, R. H. Thomas, C. C. Phillips, and I. T. Ferguson, Semicond. Sci. Technol. **8,** 101 (1993).

[33] E. O. Kane, J. Phys. Chem. Solids **1,** 249 (1957).

[34] H. Schneider and H. C. Liu, *Quantum well infrared photodetectors* (Springer, 2007).

[35] C. J. Hill, A. Soibel, D. Z. Y. Ting, S. A. Keo, J. M. Mumolo, J. Nguyen, M. Lee, and S. D. Gunapala, Electron. Lett. **45,** 1089 (2009).

[36] A. Soibel, D. Z.-Y. Ting, C. J. Hill, M. Lee, J. Nguyen, S. A. Keo, J. M. Mumolo, and S. D. Gunapala, Appl. Phys. Lett. **96,** 111102 (2010).

[37] A. Soibel, C. J. Hill, S. A. Keo, L. Hoglund, R. Rosenberg, R. Kowalczyk, A. Khoshakhlagh, A. Fisher, D. Z.-Y. Ting, and S. D. Gunapala, Appl. Phys. Lett. **105**, 023512 (2014).

Figure captions

Fig. 1 Schematic energy band structure of the three-stage ICIPs. Different absorber thickness was designed to ensure photocurrent matching between different stages.

Fig. 2 High resolution x-ray diffraction measurements for one-stage (blue) and for three-stage (red) wafers.

Fig. 3 (a) Dark current densities (b) dynamic resistance-area products as a function of bias voltage from low to high temperatures for one- and three-stage detectors. The positive voltage denotes the reverse bias, as the detectors have the reverse configuration.

Fig. 4 (a) Arrhenius plot for one- and three-stage devices with different sizes. Inset: activation energy extracted from selected devices. (b) $(R_0A)^{-1}$ *vs*. P/A for one- and three-stage devices at different temperatures. The values at 300 and 340 K had been subtracted by corresponding series resistance.

Fig. 5 (a) Responsivity under 50 mV (b) Temperature dependence of responsivity at 3.3 µm for one- and three-stage ICIPs under 0 and 50 mV bias. (c) bias dependence at various temperatures.

Fig. 6 Absorption coefficient obtained from responsivity and transmission measurements, as well as theoretical estimate based on a band model.

Fig. 7 (a) Johnson noise limited D^* at different temperatures for devices at zero-bias. (b) D* under zero-bias and a reverse bias voltage for devices at 300 K.

Figures

Figure 1

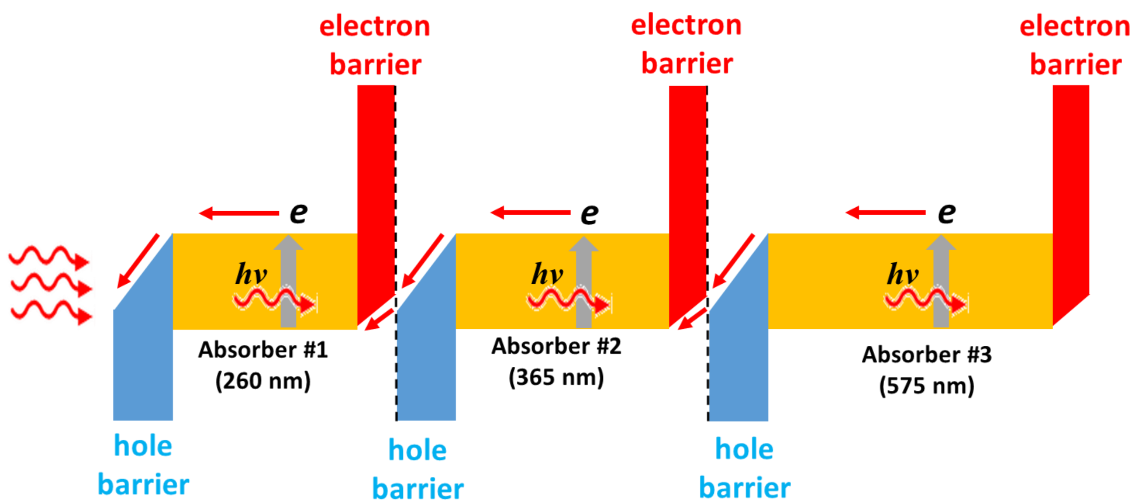

Figure 2

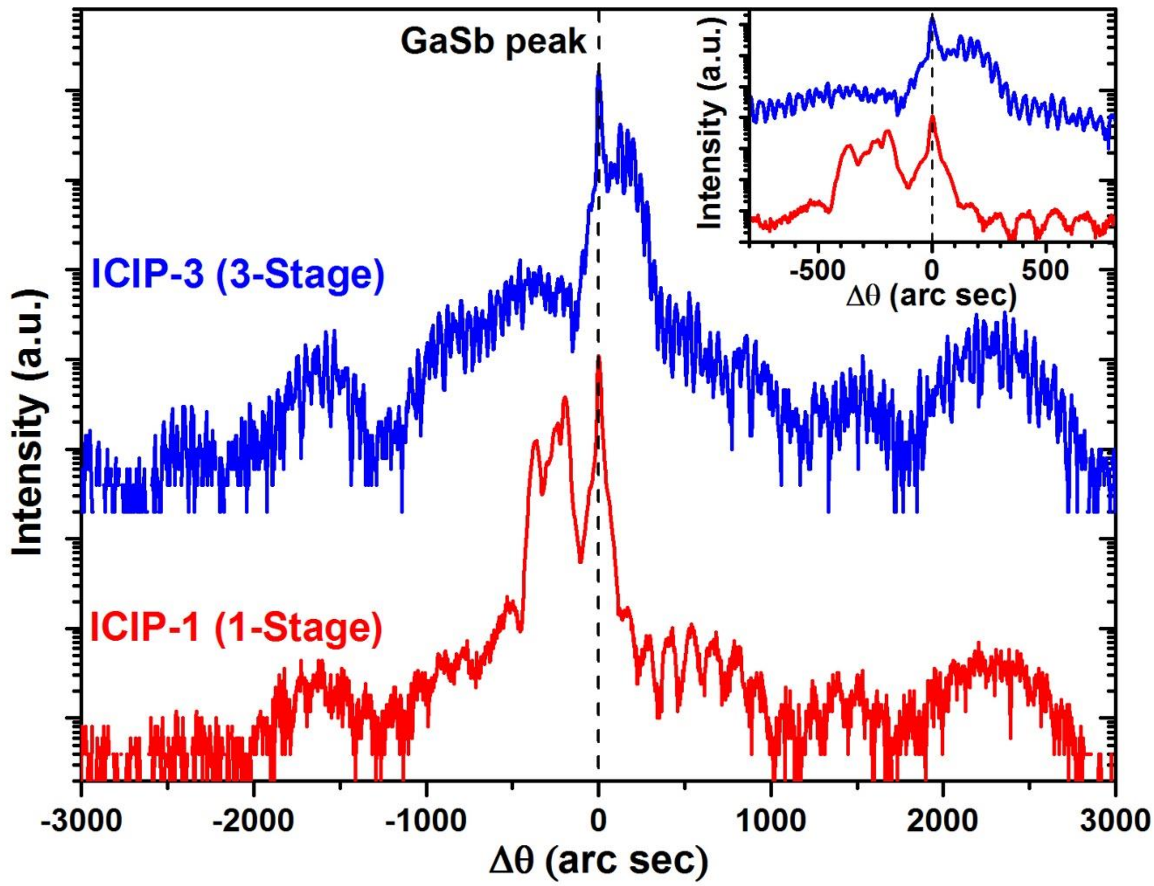
GaSb peak
ICIP-3 (3-Stage)
ICIP-1 (1-Stage)
Intensity (a.u.)
-3000
-2000
-1000
0
1000
2000
3000
Δθ (arc sec)
Intensity (a.u.)
-500
0
500
Δθ (arc sec)

Figure 3

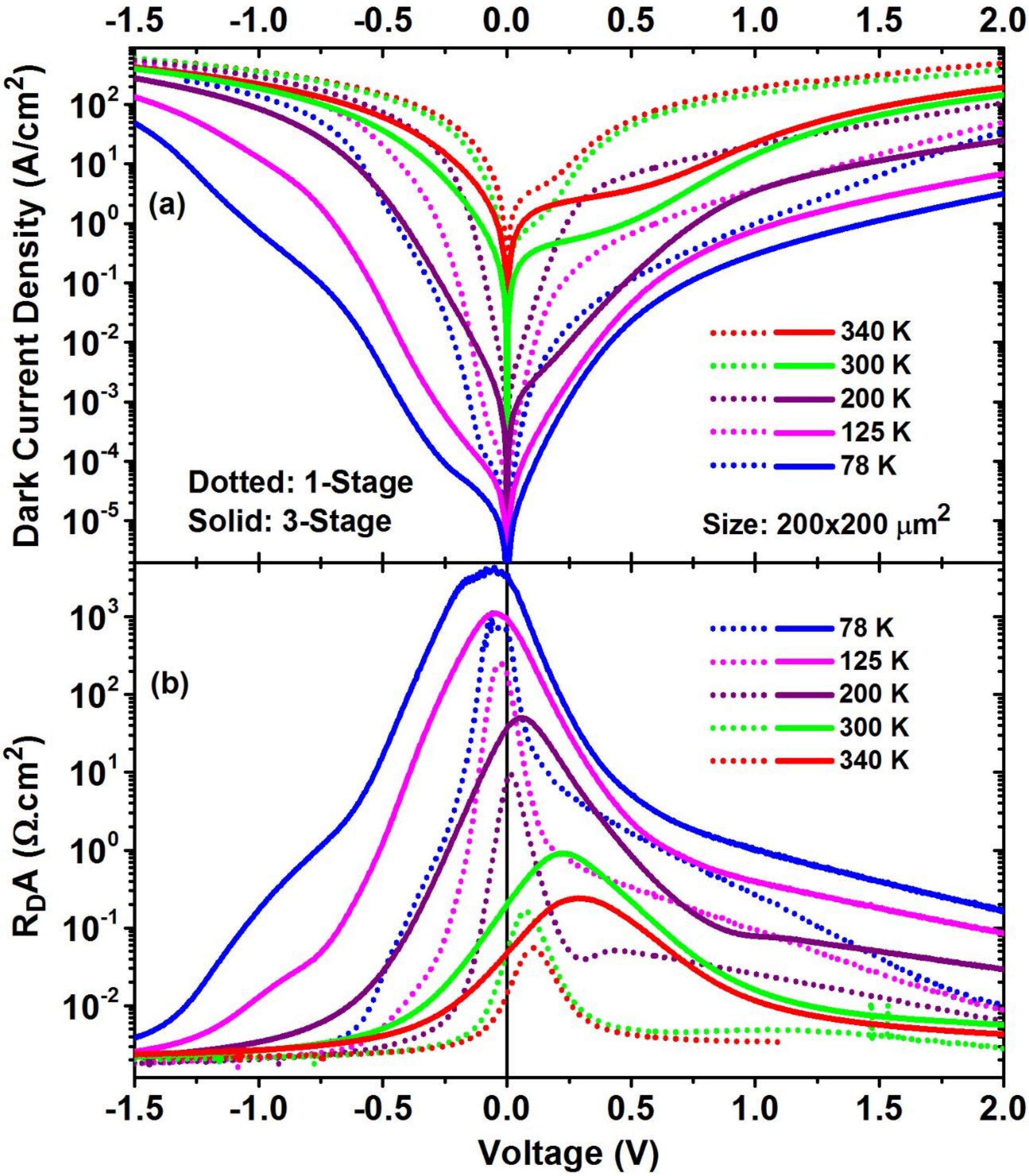

Dark Current Density (A/cm²)
(a)
Dotted: 1-Stage
Solid: 3-Stage
Size: 200x200 μm²
340 K
300 K
200 K
125 K
78 K
RDA (Ω.cm²)
(b)
78 K
125 K
200 K
300 K
340 K
Voltage (V)

Figure 4

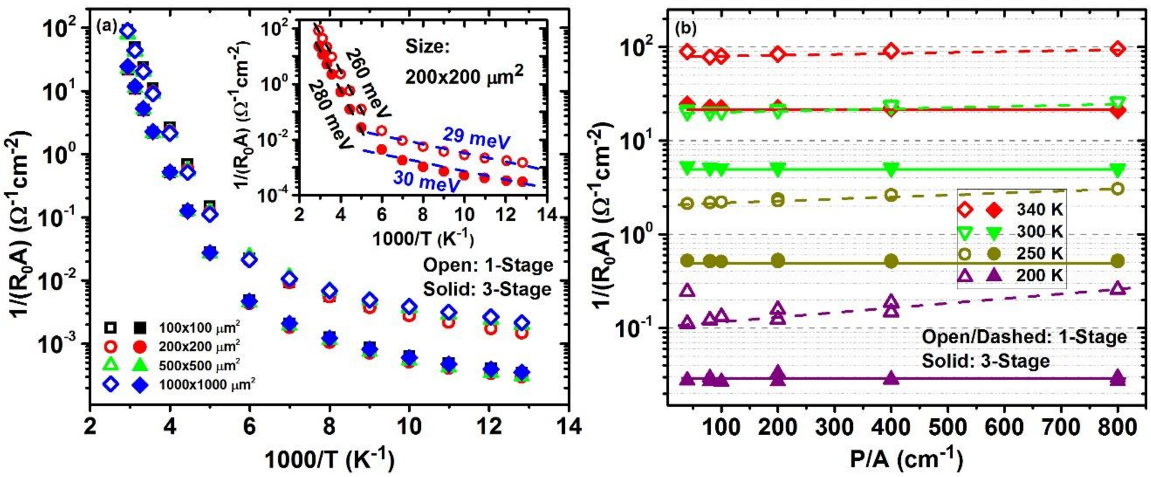
(a)
1/(R$_0$A) (Ω^{-1}cm^{-2})
1000/T (K^{-1})
Size: 200x200 μm^2
260 meV
280 meV
29 meV
30 meV
Open: 1-Stage
Solid: 3-Stage
100x100 μm^2
200x200 μm^2
500x500 μm^2
1000x1000 μm^2
(b)
340 K
300 K
250 K
200 K
Open/Dashed: 1-Stage
Solid: 3-Stage
P/A (cm^{-1})

Figure 5

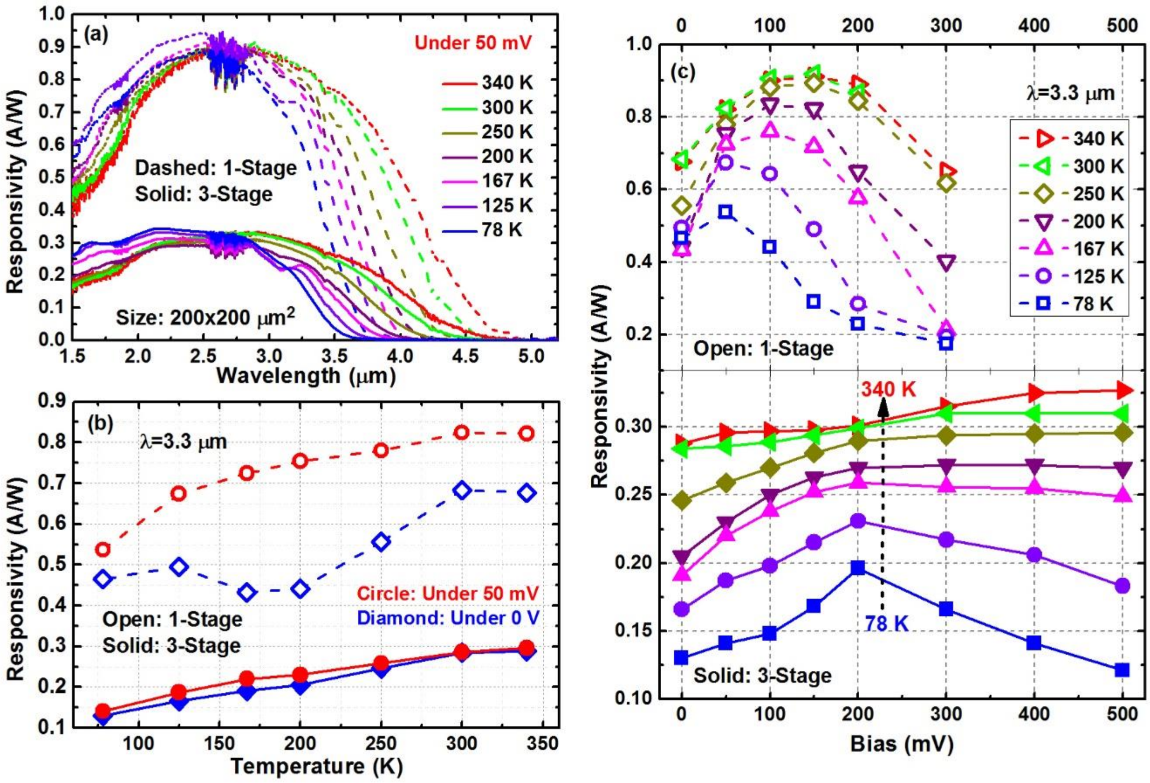
(a)
Under 50 mV
340 K
300 K
250 K
200 K
167 K
125 K
78 K
Dashed: 1-Stage
Solid: 3-Stage
Size: 200x200 μm²
Responsivity (A/W)
Wavelength (μm)
(b)
λ=3.3 μm
Circle: Under 50 mV
Diamond: Under 0 V
Open: 1-Stage
Solid: 3-Stage
Responsivity (A/W)
Temperature (K)
(c)
λ=3.3 μm
340 K
300 K
250 K
200 K
167 K
125 K
78 K
Open: 1-Stage
340 K
78 K
Solid: 3-Stage
Responsivity (A/W)
Bias (mV)

Figure 6

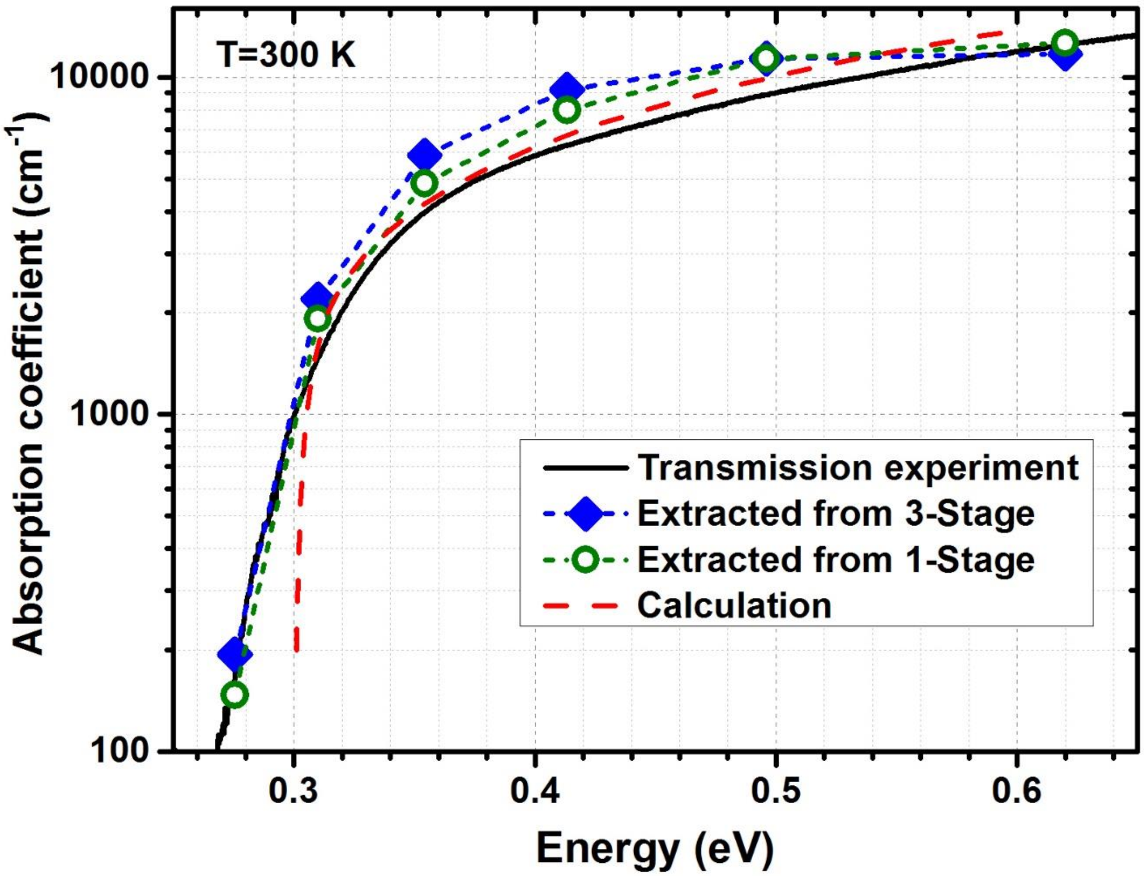
T=300 K
Absorption coefficient (cm^{-1})
10000
1000
100
0.3
0.4
0.5
0.6
Energy (eV)
Transmission experiment
Extracted from 3-Stage
Extracted from 1-Stage
Calculation

Figure 7

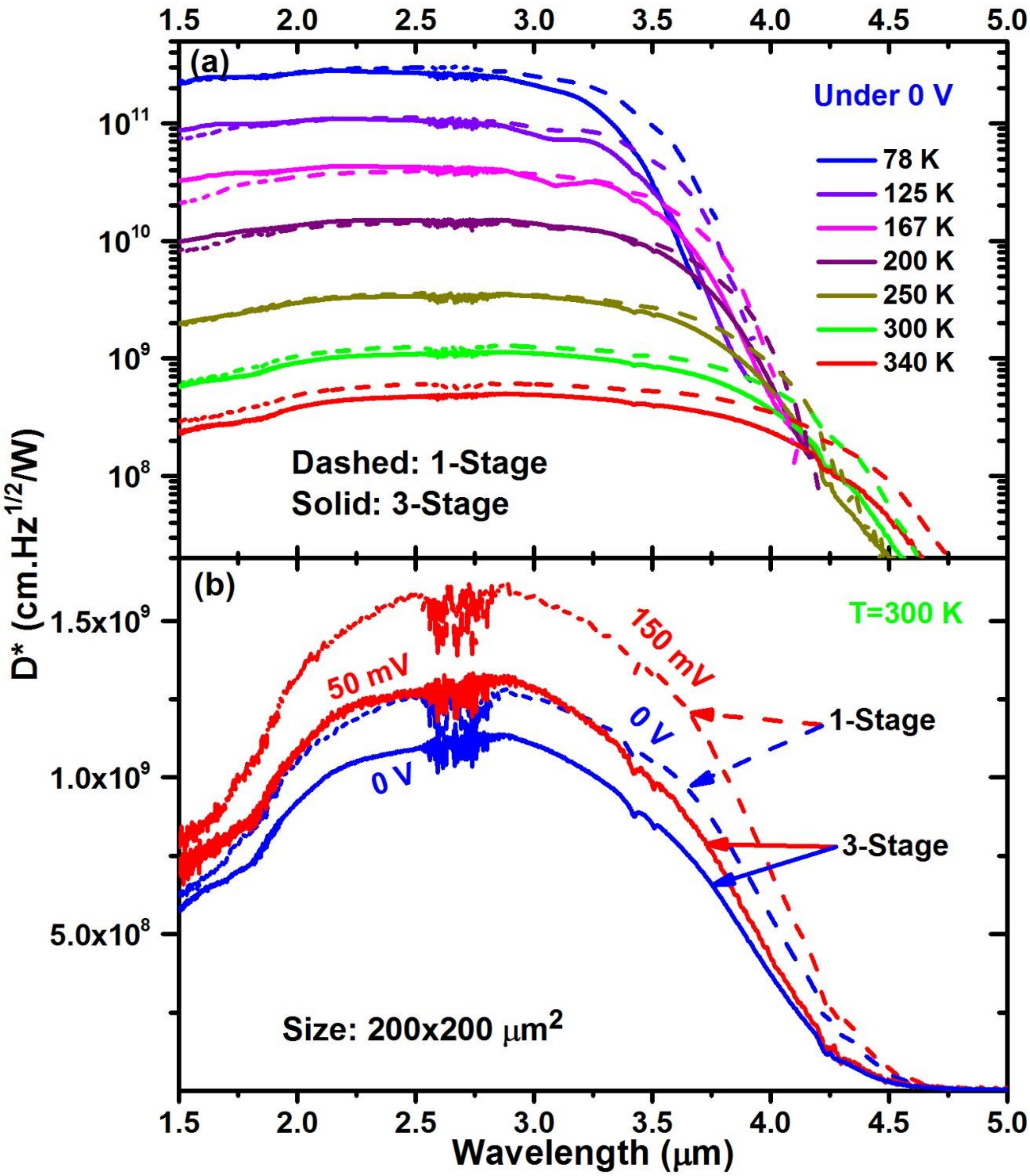
(a)
Under 0 V
78 K
125 K
167 K
200 K
250 K
300 K
340 K
Dashed: 1-Stage
Solid: 3-Stage
D* (cm.Hz^1/2/W)
(b)
T=300 K
150 mV
50 mV
0 V
0 V
1-Stage
3-Stage
Size: 200x200 μm2
Wavelength (μm)